THE JOURNAL OF PHYSICAL CHEMISTRY C
A JOURNAL OF THE AMERICAN CHEMICAL SOCIETY

pubs.acs.org/JPCC Article

SERS Detection of Charge Transfer at Electrochemical Interfaces Using Surface-Bound Ferrocene

Ruoxi Li, Imran Chaudhry, Cindy Tseng, Sizhe Weng, Yu Wang, Bofan Zhao, Indu Aravind, Zhi Cai, Jahan Dawlaty, Lasse Jensen, and Stephen B. Cronin*

Cite This: *J. Phys. Chem. C* 2023, 127, 14263−14269 Read Online

ABSTRACT: We present the novel use of surface-enhanced Raman scattering spectroscopy to detect charge transfer in ferrocene/ferrocenium (Fc/Fc^+) bound to an active electrode under electrochemical working conditions. Ferrocene has a 6-carbon linker with a thiol tether (6-(ferrocenyl)hexanethiol) and produces Fc/Fc^+ couple voltammograms exhibiting charge transfer above 0.4 V versus Ag/AgCl. By observing in situ micro-Raman spectroscopy with a water immersion lens, we observe significant changes in the spectra that correspond to the charge state oxidation of ferrocenium (Fc^+). In particular, the Fc^+ state is characterized by the disappearance of the C_p-breathing mode (1104 cm^{-1} peak) and an 11-fold increase in the hexanethiol tail mode around 1072 cm^{-1}. Raman spectra calculated by density functional theory exhibit predominant peaks that agree well with our experimental observations and indicate that the Fc → Fc^+ transition is associated with a change in the orientation, which gives rise to dramatic changes in the Raman spectra.

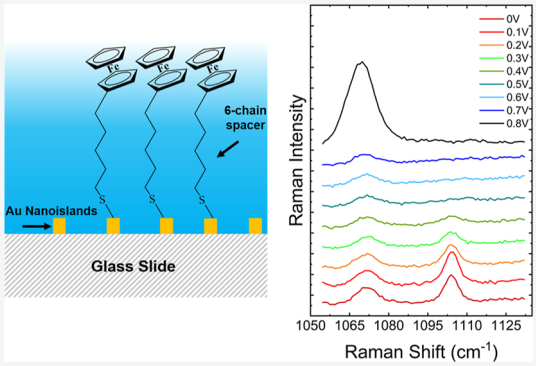

■ INTRODUCTION

Charge transfer at electrode/electrolyte interfaces is a critical step in nearly all electrocatalytic and photocatalytic processes. Much progress has been made in recent years in understanding the mechanisms and kinetics of electrocatalytic and photocatalytic systems. However, the precise potential at which charge transfer occurs is often elusive. For semiconductor photoelectrodes, the surface potential is complicated by band bending and quasi-Femi-level splitting at the semiconductor surface. Therefore, having a surface-bound molecule with a well-defined redox potential whose charge state can be monitored spectroscopically is of great interest. These so-called "charge transfer reporters" have been demonstrated using transient absorption spectroscopy but not Raman spectroscopy. Facile spectroscopic tools for studying these charge transfer events are lacking.

Electrochemical surface-enhanced Raman scattering (EC-SERS) is a powerful analytical tool that has been used for various applications, including monitoring reaction dynamics, quantifying drugs and their metabolites, and evaluating electrode materials.[1−5] EC-SERS has also been used for electrochemical cleaning, which enables sensors and detectors to be reused multiple times.[6,7] 6, 7 Several dye molecules, including Nile blue (NB) and rhodamine 6G, have been used as probe molecules in various EC-SERS studies in both aqueous and non-aqueous environments in order to investigate their adsorption behavior on different substrates, their redox activity, and their interaction with other molecules.[8,9] Our work presented here, EC-SERS, is used to provide vibrational spectra of adsorbates with a well-defined redox couple(i.e., Fc/Fc^+). Also, a detailed comparison of the experimental spectra to the theoretically calculated spectra provides clear insight into the electronic and molecular structure changes caused by electrons. This innovative approach allows for the detection of charge transfer events and surface potential spectroscopically, offering a valuable avenue to gain deeper insights into electrochemical and photoelectrochemical phenomena.

Ferrocene has been studied extensively, with more than 20,000 publications as of this writing. The use of ferrocene to study charge transfer at electrode interfaces dates back to the early 1980s.[10] As a well-defined redox couple (i.e., Fc/Fc^+), cyclic voltammetry (CV) has been used to study charge transfer at electrode surfaces.[11] Paul et al. studied the tunable redox potential and optical properties of modified ferrocene-based complexes, which span a range from +0.4 V down to −0.1 V versus SCE.[12] Smalley et al. studied the kinetics of electron transfer of ferrocene-terminated alkanethiol monolayers on gold as a function of number of methylenes in the alkyl chain tethering on gold.[13] Choudhury et al. have

Received: March 24, 2023
Revised: June 28, 2023
Published: July 13, 2023

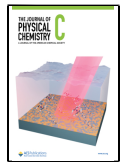

https://doi.org/10.1021/acs.jpcc.3c01973
J. Phys. Chem. C 2023, 127, 14263−14269

functionalized semiconductor surfaces with ferrocene in order to study photoexcited charge transfer.[14] Swearingen et al. reported absorption spectra showing dramatic changes in the visible range upon oxidation of ferrocene to ferrocenium, with a shift in peak absorption from ferrocene at 445 nm to ferrocenium at 619 nm.[15] Previous studies using surface-enhanced infrared absorption spectroscopy (SEIRAS) have examined Fc-terminated electrode systems as a function of electrode potential.[16,17] While these spectra lend some insight into the changes observed in the present study, it should be noted that the spectral resolution of the SEIRAS approach is at least 1 order of magnitude lower than that of Raman spectroscopy and, as such, is unable to distinguish the 2 peaks reported here (1072 and 1104 cm^{-1}).

■ METHODS

In the work presented here, SERS active electrodes are fabricated by depositing 5 nm of Au on a glass slide using electron beam deposition. These thin films of Au are not thick enough to form continuous films and instead create island-like structures that are known to be strongly plasmonic.[18−20] Figure 1b shows a high-resolution transmission electron microscopy (HRTEM) image of an Au nanoisland film with a nominal thickness of 5 nm. Figure 1c shows the electric field intensity distribution of this Au nanoisland film calculated using the finite-difference time domain (FDTD) method with a grid spacing of 2 Å.[21−23] Small gaps between the nanoislands (∼1−2 nm) dominate the optical response of these films, which produce electric field intensity "hot spots", as shown in Figure 1c. In these localized hot spot regions, the electric field intensity can be as much as 1000 times larger than the incident electric field intensity, resulting in SERS enhancement factors of 10^6.[21,24] Samples were prepared using a mixture of 10 mM 6-(ferrocenyl)hexanethiol (Sigma-Aldrich, #682527) in ethanol by soaking the substrate for 24 h. Samples are rinsed in ethanol and then immersed in an aqueous solution of 0.1 M KCl for the measurements presented in Figure 3. Figure 1a shows a diagram illustrating the SERS-active electrode, in which strips of 50 nm-thick Au are deposited on the left and right sides of the electrode, enabling electrical contact to be made to the film of Au nanoislands. Somewhat surprisingly, the plasmonic nanoislands are interconnected and provide an electrically continuous electrode with typical in-plane resistances around 100−200 Ω. We have used these plasmon-resonant nanoislands for several years for SERS spectroscopy, plasmon-enhanced catalysis, and FDTD studies of local field enhancement.[20,24−35] For the simulation, an HRTEM image of an area of 450 nm × 300 nm is used to define the spatial extent of Au nanoislands by using the Ansys Lumerical FDTD software package. A grid spacing of 2 Å is used in the volume of 500 nm × 500 nm × 40 nm around the film and 10 nm elsewhere. A temporal grid spacing of 0.002 fsec is used with a total of 100,000 time steps. A planewave source is used, which irradiates the metal film with a Gaussian pulse with a spectrum of wavelengths ranging from 300 to 800 nm. Perfectly matched layer boundary conditions are used with 25 layers. The dielectric functions of Au are based on the optical constants given by Palik.[36] In our previous work, Au nanoislands were deposited on top of monolayer graphene.[37] In this configuration, the graphene provides additional electrical continuity between the metal nanoislands. However, we have found that the graphene reduces the SERS enhancement by ∼10× and is not necessary to achieve electrical continuity within the electrode surface.

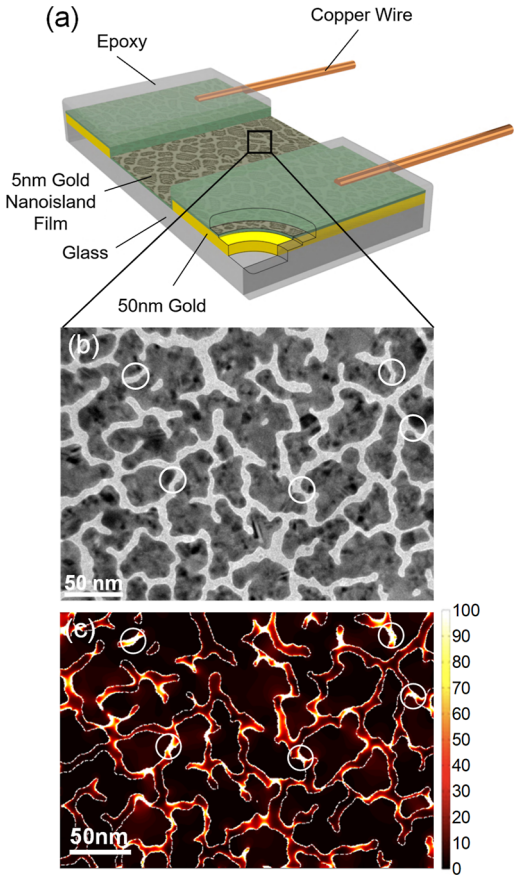

Figure 1. (a) Schematic diagram of the plasmon-resonant, SERS-active electrode fabricated with Au nanoislands. (b) TEM image and (c) FDTD simulations of the electric field distribution of the Au nanoisland film.

We measure Raman spectroscopy of electrode surfaces under working electrochemical conditions using a water immersion lens (Leica model HC APO L #506155 40×, N.A. = 0.8). Here, the SERS-active electrode shown in Figure 1 serves as the working electrode with a Pt counter electrode (26 gauge, 99.9%) and an Ag/AgCl reference electrode (BASI, MF-2052). A Gamry potentiostat (Reference 600+) is used to obtain cyclic voltammograms and apply various electrode potentials, while Raman spectra are collected using a 785 nm wavelength laser (IPS, #32912) with a Renishaw in Via micro-Raman spectrometer. Spectra are collected for 1 min of integration time with an incident laser power of 1.32 mW.

■ RESULTS AND DISCUSSION

Figure 2 shows schematic diagrams illustrating the in situ Raman spectroscopy and how sferrocene with a 6-carbon chain linker and thiol tether is deposited on the Au nanoisland films. Figure 2c shows a typical Raman spectrum of the ferrocene-functionalized, SERS-active electrode, which exhibits two sharp peaks corresponding to the C−H modes in the cyclopentadienyl rings around 1072 cm^{-1} and the C_P-breathing mode around 1104 cm^{-1}, illustrated in Figure 2d.[38] Videos illustrating the atomic motion associated with these vibrational modes are provided in the Supporting Information document.

Figure 2d shows the calculated Raman spectra of 6-(ferrocenyl)hexanethiol using the NWChem program pack-

https://doi.org/10.1021/acs.jpcc.3c01973
J. Phys. Chem. C 2023, 127, 14263−14269

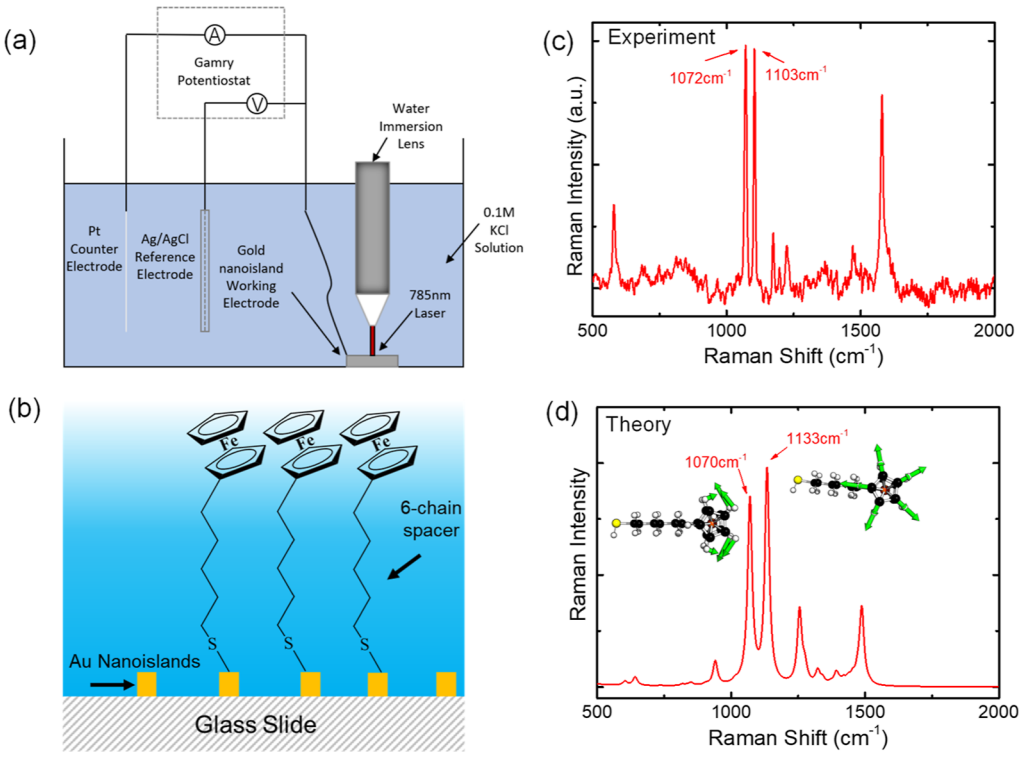

Figure 2. (a) Schematic diagram illustrating in situ Raman spectroscopy of electrode surfaces under working electrochemical conditions using a water immersion lens. (b) Cross-sectional diagram and (c) Raman spectrum of ferrocene-functionalized Au nanoisland substrate exhibiting sharp peaks corresponding to the C−H modes in the hexanethiol tail at 1072 cm^{-1} and the C_p-breathing mode around 1104 cm^{-1}. (d) DFT calculated the Raman spectrum of 6-(ferrocenyl)hexanethiol.

age.[39−41] The geometry optimizations and frequency calculations were carried out using the Becke, 3 parameter, Lee−Yang−Parr[42,43] (B3LYP) exchange−correlation functional with dispersion correction (DFT-D3) by Grimme[44] and the polarization-consistent (pc-1) basis. In Figure 2d, the predominant peaks are observed at 1069.79 and 1133.64 cm^{-1} and correspond to the C_p-scissoring and breathing modes, respectively. These vibrational frequencies are slightly different from the corresponding frequencies observed experimentally (i.e., 1072 and 1104 cm^{-1}). Nevertheless, we observe good qualitative agreement between the calculated and measured spectra. Figure S2 of the Supporting Information shows a comparison of the eclipsed ferrocene and the 6-(ferrocenyl)hexanethiol plotted over the same wavenumber range. While the 6-(ferrocenyl)hexanethiol exhibits several additional peaks not seen in the eclipsed ferrocene, the predominant peaks are observed at 1069.79 and 1133.64 cm^{-1} and correspond to the C_p-scissoring and breathing modes, respectively.

Figure 3a,b show the cyclic voltammograms (CV) taken of the ferrocene-functionalized, SERS-active electrode before and after the voltage-dependent Raman spectra plotted in Figure 3c,d. These CV curves, taken at various scan rates, exhibit clear peaks and dips corresponding to the oxidation of Fc to Fc^+ and the reduction of Fc^+ to Fc, respectively. The redox potential of this reaction is taken as the midpoint between these peaks and dips and is approximately 0.4 V versus Ag/AgCl. The Raman spectra plotted in Figure 3c,d show a clear voltage dependence that is repeatable after cycling the potential several times. Here, we see the disappearance of the C_p-breathing mode (1104 cm^{-1}) and a dramatic increase in the lower frequency mode (1072 cm^{-1}) over the applied voltage range. The peak near 1100 cm^{-1} in cycle 2 is considerably weaker than in cycle 1 at 0 V. However, the corresponding peak at 1070 cm^{-1} is quite reversible, possibly due to the fact that the cycling of the voltage entails a bond rotation that may not be fully reversible. After three cycles, however, we found that there was substantial irreversible oxidation of the surface-bound Fc. We have also included additional datasets taken on a different sample, demonstrating the reproducibility of the measurements, as plotted in Figure S4 of the Supporting Information document. Since our electrodes consist of a complex network of Au nanoislands, as shown in Figure 1, the finite series resistance between these nanoislands may contribute to the slow kinetics observed in the CV curves. Also, the compensating charge ions in solution can limit the charge transfer kinetics. Figure S6 shows CV curves taken with a continuous 50 nm−thick Au electrode, demonstrating slightly improved kinetics, although no SERS spectra could be obtained from these continuous Au film electrodes.

Figure 4 shows the calculated spectra of the 6-(ferrocenyl)-hexanethiol (Fc) and 6-(ferrocenium)hexanethiol (Fc^+). Due to the surface-selection rules in SERS, we expect that the polarizability component aligned with the strong near field will dominate the SERS spectra. The surface-selection rules lead to a strong orientation dependence in the SERS spectra. To determine a good match between the simulated and experimental spectra, we performed a search over the three principal angles: the tilt angle θ, axial rotation ϕ, and in-plane rotation χ (see diagram in Figure S1). Representative orientations are shown in Figure 4 with tilt angle θ, axial rotation ϕ, and in-plane rotation χ relative to the z-axis. Two major changes are seen in the spectra as the ferrocene is oxidized (i.e., Fc → Fc^+): (1) the spectrum shifts from two

https://doi.org/10.1021/acs.jpcc.3c01973
J. Phys. Chem. C 2023, 127, 14263−14269

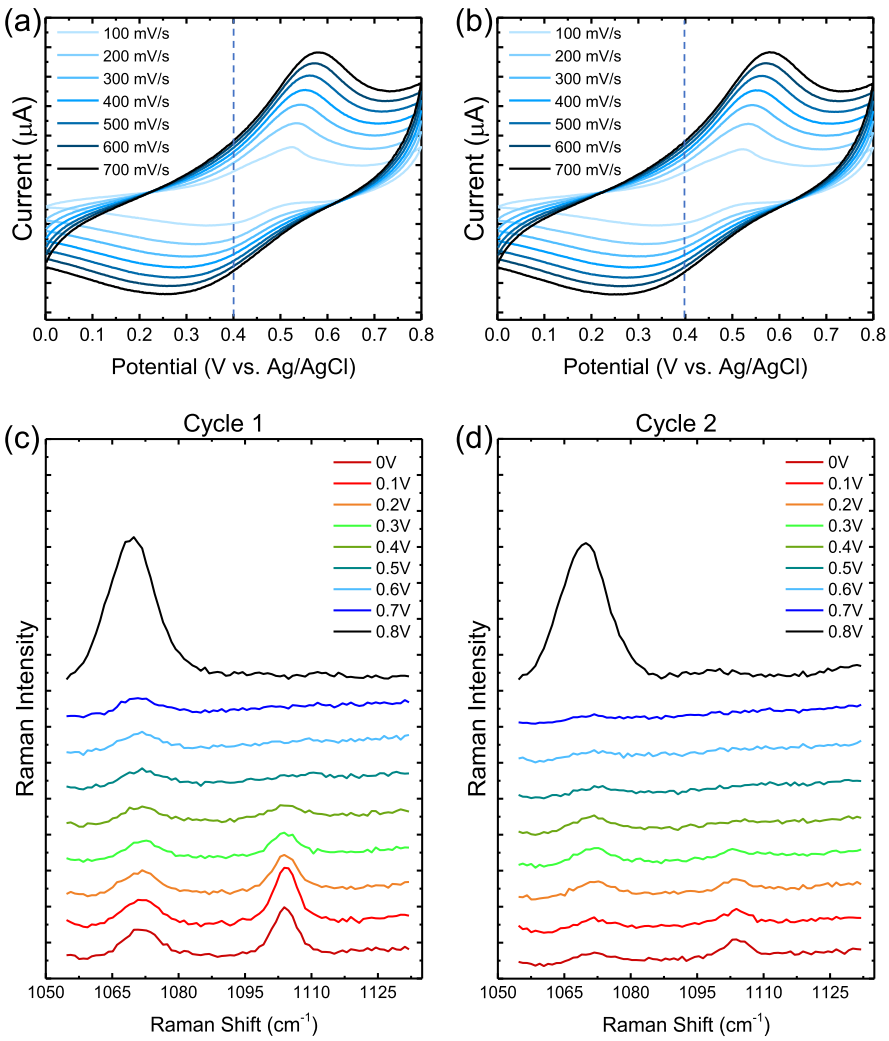

Figure 3. (a,b) Cyclic voltammograms of the ferrocene-functionalized, SERS-active electrode taken at various scan rates. (c,d) Raman spectra taken on the ferrocene-functionalized electrode under various electrode potentials vs Ag/AgCl. This data is repeatable after cycling the voltage several times.

peaks (for the Fc) to predominantly one peak (for Fc^+) in the 1050−1150 cm^{-1} range, and (2) the peak becomes centered around 1065 cm^{-1} and increases by *a* factor of 10× in intensity in the Fc^+ state. The physical mechanism corresponds to a change in the tilt angle of the molecule from $\theta = 82°$ to $\theta = 41°$ as the Fc is charged to Fc^+. Videos illustrating the atomic displacements associated with these Raman active modes [(i)/(ii) for Fc^+ and (A)/(B) for Fc] are given in the Supporting Information For the neutral Fc, the 1069 cm^{-1} Raman mode corresponds to vibrational displacements of the atoms in the ferrocene ring. However, for the cation Fc^+, the 1086/1098 cm^{-1} Raman mode corresponds to the vibrational displacements of the atoms in the hexane thiol tail of the molecule. It is important to note that there are similar modes in both molecules (Fc and Fc^+). However, due to both the change in orientation and the tail-modes being stronger in the cation, these become the dominant Raman modes in Fc^+. In addition, we measured the Raman spectra of ferrocene (without the carbon chain linker and thiol tether), as plotted in Figure S5a of the Supporting Information document. Figure S5b shows the DFT-calculated Raman spectrum of eclipsed ferrocene, which demonstrates good agreement with the experimentally measured spectrum. In the Supporting Information, we also show that charging of the Fc^+ is not sufficient to explain the observed change in the SERS spectra.

As mentioned above, several previous studies using SEIRAS have examined Fc-terminated electrodes as a function of electrode potential,[16,17] which show a significant increase in the infrared absorption around 1100 cm^{-1} due to the formation of a Fc^+/anion complex. While this increase in IR absorption stands in contrast to our observations, in which we see the disappearance of these two Raman peaks over the same range of applied electrochemical potentials, these spectra lend some insight into the changes observed in the present study. In addition to an increase in the intensity of the Fc-ring C−H stretching mode (around 1100 cm^{-1}) with increasing electrode potential, these SEIRAS studies observed a decrease in the intensity of two C−H stretching marker bands of the methylene groups, indicating that the angle between the alkyl chain and the normal to the electrode surface changes upon oxidation/reduction of the Fc moieties. The latter observation confirms an orientation change (rotation) of the ferrocene moiety.

https://doi.org/10.1021/acs.jpcc.3c01973
J. Phys. Chem. C 2023, 127, 14263−14269

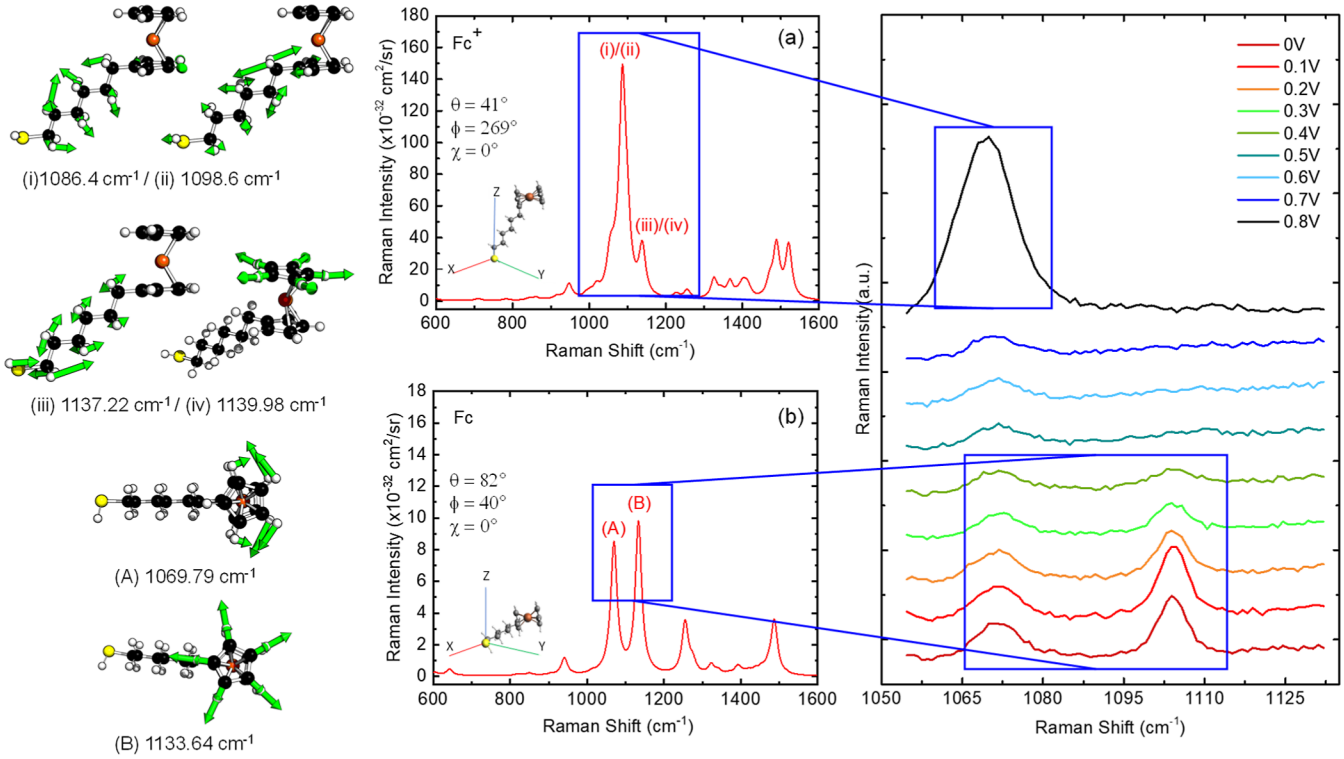

Figure 4. Calculated Raman spectra of (a) 6-(ferrocenium)hexanethiol and (b) 6-(ferrocenyl)hexanethiol.

CONCLUSIONS

In conclusion, we have demonstrated a facile technique in which commercially available ferrocene molecules are deposited on SERS-active Au electrodes and used to detect charge transfer spectroscopically. The electrochemical oxidation of Fc to Fc^+ results in a dramatic increase in the Raman intensity of the C−H mode in the hexanethiol tail and complete suppression of the C_p-breathing mode at high potentials. This general approach opens up the possibility of studying photo-initiated charge transfer and electrochemical potentials at semiconductor/liquid interfaces as well as time-resolved Raman spectroscopy using pump−probe techniques.[45,46] Raman spectra calculated by density functional theory exhibit predominant peaks that agree well with our experimental observations. While the 6-(ferrocenyl)-hexanethiol exhibits many additional peaks in the Raman spectra that are not seen in the eclipsed ferrocene, the predominant peaks are common to both molecules. The 1070 cm^{-1} mode couples to the linker and is very sensitive to the orientation of the linker. As such, the Fc → Fc^+ transition is associated with a rotation of the entire molecule, which gives rise to dramatic changes in the Raman spectra.

ASSOCIATED CONTENT

Supporting Information

The Supporting Information is available free of charge at https://pubs.acs.org/doi/10.1021/acs.jpcc.3c01973.

Schematic diagram illustrating the rotational orientation of the Fc molecule in the calculated and measured Raman spectra of eclipsed ferrocene and additional datasets taken on a different sample (PDF)

Videos illustrating the atomic vibrational modes of the neutral Fc and cation Fc^+ (ZIP)

AUTHOR INFORMATION

Corresponding Author

Stephen B. Cronin − *Department of Physics and Astronomy, Department of Chemistry, and Ming Hsieh Department of Electrical Engineering, University of Southern California, Los Angeles, California 90089, United States;* orcid.org/0000-0001-9153-7687; Email: scronin@usc.edu

Authors

Ruoxi Li − *Mork Family Department of Chemical Engineering and Materials Science, University of Southern California, Los Angeles, California 90089, United States;* orcid.org/0000-0002-6432-6072

Imran Chaudhry − *Department of Chemistry, Pennsylvania State University, University Park, Pennsylvania 16802, United States*

Cindy Tseng − *Department of Chemistry, University of Southern California, Los Angeles, California 90089, United States*

Sizhe Weng − *Ming Hsieh Department of Electrical Engineering, University of Southern California, Los Angeles, California 90089, United States*

Yu Wang − *Mork Family Department of Chemical Engineering and Materials Science, University of Southern California, Los Angeles, California 90089, United States;* orcid.org/0000-0002-0307-1301

Bofan Zhao − *Ming Hsieh Department of Electrical Engineering, University of Southern California, Los Angeles, California 90089, United States;* orcid.org/0000-0003-0478-6330

Indu Aravind − *Department of Physics and Astronomy, University of Southern California, Los Angeles, California 90089, United States*

https://doi.org/10.1021/acs.jpcc.3c01973
J. Phys. Chem. C 2023, 127, 14263−14269

Zhi Cai − *Mork Family Department of Chemical Engineering and Materials Science, University of Southern California, Los Angeles, California 90089, United States;* orcid.org/0000-0002-3741-5715

Jahan Dawlaty − *Department of Chemistry, University of Southern California, Los Angeles, California 90089, United States;* orcid.org/0000-0001-5218-847X

Lasse Jensen − *Department of Chemistry, Pennsylvania State University, University Park, Pennsylvania 16802, United States;* orcid.org/0000-0003-1237-5021

Complete contact information is available at: https://pubs.acs.org/10.1021/acs.jpcc.3c01973

Notes

The authors declare no competing financial interest.

■ ACKNOWLEDGMENTS

This research was supported by the U.S. Department of Energy, Office of Basic Energy Sciences award no. DESC0019322 (R.L.); the Army Research Office (ARO) award no. W911NF-22-1−0284 (Y.W.); National Science Foundation (NSF) award nos. CHE-2106151 (I.C. and L.J.), CHE-2106480 (S.W.), CBET-2012845 (Z.C.), and CBET-1954834 (I.A.); and Air Force Office of Scientific Research (AFOSR) grant no. FA9550-19-1-0115 (B.Z.).

■ REFERENCES

(1) Maduraiveeran, G.; Jin, W. Nanomaterials based electrochemical sensor and biosensor platforms for environmental applications. *Trends Environ. Anal. Chem.* **2017**, *13*, 10−23.

(2) Xiao, T.; Huang, J.; Wang, D.; Meng, T.; Yang, X. Au and Au-Based nanomaterials: Synthesis and recent progress in electrochemical sensor applications. *Talanta* **2020**, *206*, 120210.

(3) Huang, Z.; Zhang, A.; Zhang, Q.; Cui, D. Nanomaterial-based SERS sensing technology for biomedical application. *J. Mater. Chem. B* **2019**, *7*, 3755−3774.

(4) Yuan, Y.; Panwar, N.; Yap, S. H. K.; Wu, Q.; Zeng, S.; Xu, J.; Tjin, S. C.; Song, J.; Qu, J.; Yong, K.-T. SERS-based ultrasensitive sensing platform: An insight into design and practical applications. *Coord. Chem. Rev.* **2017**, *337*, 1−33.

(5) Moldovan, R.; Vereshchagina, E.; Milenko, K.; Iacob, B.-C.; Bodoki, A. E.; Falamas, A.; Tosa, N.; Muntean, C. M.; Farcău, C.; Bodoki, E. Review on combining surface-enhanced Raman spectroscopy and electrochemistry for analytical applications. *Anal. Chim. Acta* **2022**, *1209*, 339250.

(6) Hu, Y.; Wu, C.; Huang, S.; Luo, X.; Yuan, R.; Yang, X. A novel SERS substrate with high reusability for sensitive detection of miRNA 21. *Talanta* **2021**, *228*, 122240.

(7) Tsai, M.-H.; Lin, Y.-K.; Luo, S.-C. Electrochemical SERS for in situ monitoring the redox states of PEDOT and its potential application in oxidant detection. *ACS Appl. Mater. Interfaces* **2018**, *11*, 1402−1410.

(8) Wilson, A. J.; Molina, N. Y.; Willets, K. A. Modification of the electrochemical properties of Nile Blue through covalent attachment to gold as revealed by electrochemistry and SERS. *J. Phys. Chem. C* **2016**, *120*, 21091−21098.

(9) Zaleski, S.; Cardinal, M. F.; Klingsporn, J. M.; Van Duyne, R. P. Observing single, heterogeneous, one-electron transfer reactions. *J. Phys. Chem. C* **2015**, *119*, 28226−28234.

(10) Gagne, R. R.; Koval, C. A.; Lisensky, G. C. Ferrocene as an Internal Standard for Electrochemical Measurements. *Inorg. Chem.* **1980**, *19*, 2854−2855.

(11) Alehashem, S.; Chambers, F.; Strojek, J. W.; Swain, G. M.; Ramesham, R. Cyclic Voltammetric Studies of Charge-Transfer Reactions at Highly Boron-Doped Polycrystalline Diamond Thin-Film Electrodes. *Anal. Chem.* **1995**, *67*, 2812−2821.

(12) Paul, A.; Borrelli, R.; Bouyanfif, H.; Gottis, S.; Sauvage, F. Tunable Redox Potential, Optical Properties, and Enhanced Stability of Modified Ferrocene-Based Complexes. *Acs Omega* **2019**, *4*, 14780−14789.

(13) Smalley, J. F.; Feldberg, S. W.; Chidsey, C. E. D.; Linford, M. R.; Newton, M. D.; Liu, Y. P. The Kinetics of Electron-Transfer through Ferrocene-Terminated Alkanethiol Monolayers on Gold. *J. Phys. Chem.* **1995**, *99*, 13141−13149.

(14) Choudhury, M. H.; Ciampi, S.; Lu, X. Y.; Kashi, M. B.; Zhao, C.; Gooding, J. J. Spatially confined electrochemical activity at a non-patterned semiconductor electrode. *Electrochim Acta* **2017**, *242*, 240−246.

(15) Swearingen, C.; Wu, J.; Stucki, J.; Fitch, A. Use of ferrocenyl surfactants of varying chain lengths to study electron transfer reactions in native montmorillonite clay. *Environ. Sci. Technol.* **2004**, *38*, 5598−603.

(16) Rudnev, A. V.; Zhumaev, U.; Utsunomiya, T.; Fan, C. J.; Yokota, Y.; Fukui, K.; Wandlowski, T. Ferrocene-terminated alkanethiol self-assembled monolayers: An electrochemical and in situ surface-enhanced infra-red absorption spectroscopy study. *Electrochim Acta* **2013**, *107*, 33−44.

(17) Tu, K. Y.; Morhart, T. A.; Read, S. T.; Rosendahl, S. M.; Burgess, I. J. Probing Heterogeneity in Attenuated Total Reflection Surface-Enhanced Infrared Absorption Spectroscopy (ATR-SEIRAS) Response with Synchrotron Infrared Microspectroscopy. *Appl. Spectrosc.* **2021**, *75*, 1198−1206.

(18) Kumar, R.; Zhou, H.; Cronin, S. B. Surface-enhanced Raman spectroscopy and correlated scanning electron microscopy of individual carbon nanotubes. *Appl. Phys. Lett.* **2007**, *91*, 223105.

(19) Kneipp, K.; Kneipp, H.; Corio, P.; Brown, S. D. M.; Shafer, K.; Motz, J.; Perelman, L. T.; Hanlon, E. B.; Marucci, A.; Dresselhaus, G.; et al. Surface-enhanced and normal Stokes and anti-Stokes Raman spectroscopy of single-walled carbon nanotubes. *Phys. Rev. Lett.* **2000**, *84*, 3470−3473.

(20) Liu, Z.; Hou, W.; Pavaskar, P.; Aykol, M.; Cronin, S. Plasmon Resonant Enhancement of Photocatalytic Water Splitting Under Visible Illumination. *Nano Lett.* **2011**, *11*, 1111−1116.

(21) Pavaskar, P.; Theiss, J.; Cronin, S. B. Plasmonic hot spots: nanogap enhancement vs. focusing effects from surrounding nanoparticles. *Opt Express* **2012**, *20*, 14656−14662.

(22) Pavaskar, P.; Hsu, I. K.; Theiss, J.; Hsuan Hung, W.; Cronin, S. B. A microscopic study of strongly plasmonic Au and Ag island thin films. *J. Appl. Phys.* **2013**, *113*, 034302.

(23) Pavaskar, P.; Cronin, S. B. Iterative optimization of plasmon resonant nanostructures. *Appl. Phys. Lett.* **2009**, *94*, 253102.

(24) Pavaskar, P.; Hsu, I. K.; Theiss, J.; Hsuan Hung, W.; Cronin, S. B. A microscopic study of strongly plasmonic Au and Ag island thin films. *J. Appl. Phys.* **2013**, *113*, 034302.

(25) Chen, J.; Bailey, C. S.; Hong, Y.; Wang, L.; Cai, Z.; Shen, L.; Hou, B.; Wang, Y.; Shi, H.; Sambur, J.; et al. Plasmon-Resonant Enhancement of Photocatalysis on Monolayer WSe2. *ACS Photonics* **2019**, *6*, 787−792.

(26) Hao, E.; Schatz, G. C. Electromagnetic fields around silver nanoparticles and dimers. *J. Chem. Phys.* **2004**, *120*, 357−66.

(27) Hou, W.; Cronin, S. B. A Review of Surface Plasmon Resonance-Enhanced Photocatalysis. *Adv. Funct. Mater.* **2013**, *23*, 1612−1619.

(28) Hou, W.; Hung, W. H.; Pavaskar, P.; Goeppert, A.; Aykol, M.; Cronin, S. B. Photocatalytic Conversion of CO2 to Hydrocarbon Fuels via Plasmon-Enhanced Absorption and Metallic Interband Transitions. *ACS Catal.* **2011**, *1*, 929−936.

(29) Hou, W.; Liu, Z.; Pavaskar, P.; Hung, W. H.; Cronin, S. B. Plasmonic enhancement of photocatalytic decomposition of methyl orange under visible light. *J. Catal.* **2011**, *277*, 149−153.

(30) Hung, W. H.; Aykol, M.; Valley, D.; Hou, W.; Cronin, S. B. Plasmon resonant enhancement of carbon monoxide catalysis. *Nano Lett.* **2010**, *10*, 1314−8.

(31) Hung, W. H.; Hsu, I. K.; Bushmaker, A.; Kumar, R.; Theiss, J.; Cronin, S. B. Laser directed growth of carbon-based nanostructures

by plasmon resonant chemical vapor deposition. *Nano Lett.* **2008**, *8*, 3278−82.
(32) Lin, J. J.; Shen, J. X.; Wang, R. J.; Cui, J. J.; Zhou, W. J.; Hu, P. G.; Liu, D. O.; Liu, H.; Wang, J. Y.; Boughton, R. I.; et al. Nano-p-n junctions on surface-coarsened TiO_2 nanobelts with enhanced photocatalytic activity. *J. Mater. Chem.* **2011**, *21*, 5106−5113.
(33) Pavaskar, P.; Theiss, J.; Cronin, S. B. Plasmonic hot spots: nanogap enhancement vs. focusing effects from surrounding nanoparticles. *Opt Express* **2012**, *20*, 14656−62.
(34) Qiu, J.; Zeng, G.; Pavaskar, P.; Li, Z.; Cronin, S. B. Plasmon-enhanced water splitting on TiO2-passivated GaP photocatalysts. *Phys. Chem. Chem. Phys.* **2014**, *16*, 3115−3121.
(35) Zhang, J.; Wang, G.; Wang, T.; Li, F. Genetic algorithms to automate the design of metasurfaces for absorption bandwidth broadening. *ACS Appl. Interfaces* **2021**, *13*, 7792−7800.
(36) Palik, E. D. *Handbook of Optical Constants of Solids*; Academic ress, 1998; Vol. 3.
(37) Shi, H.; Cai, Z.; Patrow, J.; Zhao, B.; Wang, Y.; Wang, Y.; Benderskii, A.; Dawlaty, J.; Cronin, S. B. Monitoring Local Electric Fields at Electrode Surfaces Using Surface Enhanced Raman Scattering-Based Stark-Shift Spectroscopy during Hydrogen Evolution Reactions. *ACS Appl. Interfaces* **2018**, *10*, 33678−33683.
(38) Shimei, J.; Yue, W. Vibrational spectra of an open ferrocene and a half-open ferrocene. *Spectrochim. Acta, Part A* **1999**, *55*, 1025−1033.
(39) te Velde, G.; Bickelhaupt, F. M.; Baerends, E. J.; Fonseca Guerra, C.; Van Gisbergen, S. J. A.; Snijders, J. G.; Ziegler, T. Chemistry with ADF. *J. Comput. Chem.* **2001**, *22*, 931−967.
(40) Fonseca Guerra, C.; Snijders, J. G.; te Velde, G.; Baerends, E. J. Towards an order-N DFT method. *Theor. Chem. Acc.* **1998**, *99*, 391−403.
(41) Baerends, E. J.; et al. ADF. *Theoretical Chemistry*; Vrije Universiteit: Amsterdam, The Netherlands, 2019.
(42) Becke, A. D. Density-Functional Exchange-Energy Approximation with Correct Asymptotic-Behavior. *Phys. Rev. A: At., Mol., Opt. Phys.* **1988**, *38*, 3098−3100.
(43) Perdew, J. P. Density-Functional Approximation for the Correlation-Energy of the Inhomogeneous Electron-Gas. *Phys. Rev. B: Condens. Matter Mater. Phys.* **1986**, *33*, 8822−8824.
(44) Grimme, S.; Ehrlich, S.; Goerigk, L. Effect of the Damping Function in Dispersion Corrected Density Functional Theory. *J. Comput. Chem.* **2011**, *32*, 1456−1465.
(45) Frontiera, R. R.; Mathies, R. A. Femtosecond stimulated Raman spectroscopy. *Laser Photon. Rev.* **2011**, *5*, 102−113.
(46) Frontiera, R. R.; Henry, A. I.; Gruenke, N. L.; Van Duyne, R. P. Surface-Enhanced Femtosecond Stimulated Raman Spectroscopy. *J. Phys. Chem. Lett.* **2011**, *2*, 1199−1203.

https://doi.org/10.1021/acs.jpcc.3c01973
J. Phys. Chem. C 2023, 127, 14263−14269